Spin-valley relaxation and quantum transport regimes in two-dimensional transition-metal dichalcogenides

Hector Ochoa,[1,2] Francesca Finocchiaro,[1] Francisco Guinea,[1,3] and Vladimir I. Fal'ko[4]
[1]*Instituto de Ciencia de Materiales de Madrid, CSIC, 28049 Madrid, Spain*
[2]*Donostia International Physics Center (DIPC), 20018 San Sebastián, Spain*
[3]*School of Physics and Astronomy, University of Manchester, Oxford Road, Manchester, M13 9PL, United Kingdom*
[4]*Physics Department, Lancaster University, Lancaster, LA1 4YB, United Kingdom*
(Received 9 August 2014; revised manuscript received 19 November 2014; published 22 December 2014)

Quantum transport and spintronics regimes are studied in p- and n-doped atomic layers of hexagonal transition-metal dichalcogenides (TMDCs), subject to the interplay between the valley structure and spin-orbit coupling. We find how spin relaxation of carriers depends on their areal density and show that it vanishes for holes near the band edge, leading to the density-independent spin-diffusion length, and we develop a theory of weak localization/antilocalization, describing the crossovers between the orthogonal, double-unitary, and symplectic regimes of quantum transport in TMDCs.

DOI: 10.1103/PhysRevB.90.235429 PACS number(s): 73.23.−b, 72.15.Rn, 72.25.Rb

I. INTRODUCTION

Among the novel two-dimensional materials that have attracted a lot of attention during the recent years, semiconducting transition-metal dichalcogenides (TMDCs) [1] are particularly interesting due to their potential for applications in electronics and optoelectronics [2–6]. They have been recently implemented in field-effect transistors [7–14], showing large in-plane mobilities and a high current on/off ratio, which make them also very interesting for sensors. This has motivated a big effort in the study of the transport properties of these single-layer crystals [15–20].

Contrary to their bulk counterparts, single-layer TMDCs are considered to have a direct band gap [21], which appears at the corners $K_\pm$ of the hexagonal Brillouin zone (see Fig. 1). Simultaneously, the large spin-orbit (SO) interaction provided by the heavy transition-metal atoms together with the lack of inversion symmetry splits the energy bands around $K_\pm$ points [22–29], where the out-of-plane spin polarization is still a good quantum number due to the mirror symmetry ($z \to -z$) of the system. The interplay between valley and spin degrees of freedom influences charge and spin transport characteristics of these materials. In general, magnetotransport experiments in systems with large SO coupling provide insights about the nature of momentum scattering and spin relaxation processes, whereas the interplay between spin-lattice relaxation and quantum transport leads to a crossover between orthogonal and symplectic classes of quantum disordered systems [30,31], manifested in measurements as weak localization [32] (WL) and weak antilocalization [33] (WAL) magnetoresistance (MR). This interplay acquires an additional twist in two-dimensional (2D) conductors with a multivalley band structure [34–38]. In the case of TMDCs, the SO spin splitting tends to suppress spin relaxation, whereas lattice defects and deformations mimic time-inversion symmetry breaking for the intravalley propagation of carriers (although the true time-inversion symmetry is preserved because it involves interchanging the valleys).

In this work, we study in detail the interplay between SO coupling and multivalley properties in spintronics and quantum transport of single-layer TMDCs. We identify three regimes of quantum transport, which are distinguished by the relative size of the SO splitting and the Fermi energy of charge carriers, as sketched in Fig. 1. The structure of the paper is the following: In Sec. II, we present the phenomenological model for TMDCs band structure and disorder, supported by $\mathbf{k}\cdot\mathbf{p}$ theory derivation in Appendices A and B. In Sec. III, we analyze the interference correction to the conductivity and show that it displays various forms of the WL to WAL crossover, depending on the relation between the spin splitting and Fermi energy of the carriers. In Sec. IV, we discuss the occurrence of such crossovers in, e.g., MoS_2.

II. MODEL

Two-dimensional unit cells of TMDCs consist on X-M-X layers, where the transition-metal atoms (M) are ordered in a triangular lattice, each of them bonded to six chalcogen atoms (X) located in the top and bottom layers (see Fig. 1). We focus on the dynamics of spinful electrons and holes around the $K_\pm$ valleys. To that end, we introduce Pauli algebras associated to valley (τ matrices) and spin (s matrices), which can be classified according to the irreducible representations of D_{3h}'' (see Table I). Here, we deal with D_{3h}'', the point group associated to the tripled unit cell, because it allows us to treat excitations at both valleys on an equal footing (see Appendix A).

The $\mathbf{k}\cdot\mathbf{p}$ theory Hamiltonian for electrons and holes in TMDCs has the form [23–25,39–42]

$$\mathcal{H} = \frac{|\mathbf{p}|^2}{2m^*} + \mu\left(p_x^3 - 3p_x p_y^2\right)\tau_z + \frac{\lambda}{2}\tau_z s_z + \delta\mathcal{H}(\mathbf{r}). \quad (1a)$$

This takes into account trigonal warping μ of their dispersion inverted in $K_\pm$ valleys and SO splitting λ [large (small) in the valence (conduction) band (see Table II)]. The last term in Eq. (1a),

$$\begin{aligned}\delta\mathcal{H}(\mathbf{r}) = {} & u_0(\mathbf{r}) + u_z(\mathbf{r})\tau_z s_z + \{\mathbf{p},\mathbf{a}_g(\mathbf{r})\}\tau_z + \{\mathbf{p},\mathbf{a}_{gz}(\mathbf{r})\}s_z \\ & + \mathbf{u}_{sf}(\mathbf{r})\cdot\mathbf{s}\tau_z + \sum_{\alpha=x,y}\{\mathbf{p},\mathbf{w}_\alpha(\mathbf{r})\}s_\alpha + \mathbf{u}_i(\mathbf{r})\cdot\boldsymbol{\tau} \\ & + \sum_{\alpha=x,y}\{\mathbf{p},\mathbf{w}_{z\alpha}\}\tau_\alpha s_z + \sum_{\alpha,\beta=x,y}\{\mathbf{p},\mathbf{w}_{\alpha\beta}\}\tau_\alpha s_\beta, \quad (1b)\end{aligned}$$

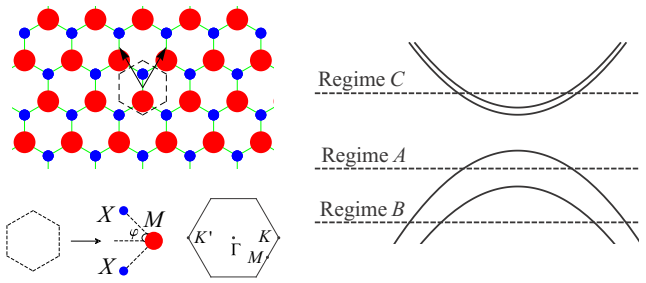

FIG. 1. (Color online) Left: lattice, unit cell, and Brillouin zone of TMDC monolayers. Right: schematic view of the quantum transport regimes discussed through the text.

describes imperfections in the 2D crystal that, in principle, break all its symmetries except for time reversal.

The first two terms in $\delta\mathcal{H}(\mathbf{r})$ stand for intravalley disorder, sensitive to the allowed spin state of the electron in each valley. The next two terms account for both lattice deformations (responsible for a valley-/spin-dependent pseudomagnetic field [34,35]) and the Berry curvature specific for the bands at the corners of the Brillouin zone. Their $\mathbf{k}\cdot\mathbf{p}$ theory [25] derivation is described in Appendix B. The presence of the last two terms in the first line, with spin operators $(s_x,s_y)\equiv\mathbf{s}$, requires $z\to -z$ symmetry breaking, e.g., by flexural deformations of the 2D crystal in the case of the last term [43].

The second line in Eq. (1b), with valley Pauli matrices $(\tau_x,\tau_y)\equiv\boldsymbol{\tau}$, describes intervalley disorder due to atomic defects in the crystal. The first two terms account for intervalley scattering without spin flip; the last term represents the only intervalley spin-flip perturbation permitted by the time-inversion symmetry in the lowest-order $\mathbf{k}\cdot\mathbf{p}$ expansion around $K_\pm$. The momentum dependence of such a term suggests that the intervalley spin-flip scattering is absent for the carriers at the band edge [44,45].

III. QUANTUM TRANSPORT REGIMES

We study the phase-coherent quantum interference correction to conductivity since the typical mean-free paths deduced from the mobilities reported in monolayers of TMDCs (see Table II) are of the order of $\ell\sim$ 1–10 nm, whereas the phase-coherence lengths reported in magnetotransport experiments in few-layer samples are of the order of $\ell_\varphi\sim$ 50–100 nm [46,47]. The analysis of quantum transport characteristics of TMDCs is based on the diagrammatic perturbation theory calculations similar to those performed earlier in graphene [36,37,48] and other 2D materials [38]. Depending on the relative size of SO splitting and Fermi energy ε_F of charge carriers (see Fig. 1), we identify three distinct spin/valley relaxation and quantum transport regimes:

(A) $\boldsymbol{\lambda > \varepsilon_F}$: lightly p-doped monolayers of MoX_2 and WX_2 (X = S, Se, Te) with holes fully spin polarized in opposite directions in the opposite valleys [26–29].

(B) $\boldsymbol{\varepsilon_F \gtrsim \lambda}$: specific for heavily p-doped MoS_2.

(C) $\boldsymbol{\varepsilon_F \gg \lambda}$: typical for n-doped MoX_2 monolayers.

TABLE I. Definitions of valley and spin matrices.

Irrep	$t\to -t$ invariant	$t\to -t$ odd
A_2'		τ_z, s_z
E''		$\begin{pmatrix}s_x\\ s_y\end{pmatrix}$
$E_{1,2}'$	$\begin{pmatrix}\tau_x\\ \tau_y\end{pmatrix}$	

A. Regime A: $\lambda > \epsilon_F$ (valence band)

Energy conservation and spin polarization of electrons in opposite directions ($\uparrow\downarrow$) in valleys $K_\pm$ do not leave any space for intravalley spin-flip and intervalley spin-conserving scatterings. This makes redundant the last two terms in the first line of Eq. (1b) and first two terms in the second line. Then, spin-conserving intravalley disorder is characterized by the scattering rate

$$\tau_0^{-1}=\frac{2\pi\nu(\Omega_0+\Omega_z)}{\hbar},\quad \nu=\frac{m^*}{2\pi\hbar^2},$$
$$\langle u_\alpha(\mathbf{r})u_\beta(\mathbf{r}')\rangle=\Omega_\alpha\delta_{\alpha\beta}\delta(\mathbf{r}-\mathbf{r}'),\quad \alpha=(0,z). \tag{2a}$$

The gauge-field-like part of $\delta\mathcal{H}$ determines the rate

$$\tau_g^{-1}=\frac{2\pi\nu p_F^2(\Theta_g+\Theta_{gz})}{\hbar}\propto n_h,$$
$$\left\langle a_\alpha^i(\mathbf{r})a_\beta^j(\mathbf{r}')\right\rangle=\Theta_\alpha\delta_{\alpha\beta}\delta_{ij}\delta(\mathbf{r}-\mathbf{r}'),\quad \alpha=(g,gz) \tag{2b}$$

which scale linearly with the hole density n_h. The last term in Eq. (1b), with $(\alpha,\beta=x,y)$ is responsible for the only possible intervalley scattering process in the regime A, accompanied by a spin flip, which determines the hole spin relaxation rate [44]

$$\tau_{is}^{-1}=\frac{8\pi\nu p_F^2\Theta_{is}}{\hbar}\propto n_h,$$
$$\left\langle w_{\alpha\beta}^i(\mathbf{r})w_{\alpha'\beta'}^j(\mathbf{r}')\right\rangle=\Theta_{is}\delta_{\alpha\alpha'}\delta_{\beta\beta'}\delta_{ij}\delta(\mathbf{r}-\mathbf{r}'), \tag{2c}$$

which also scales linearly with the hole density.

Rates (2) sum up into the momentum relaxation rate

$$\tau^{-1}=\tau_0^{-1}+\tau_g^{-1}+\tau_{is}^{-1},$$

which determines the value of Drude conductivity and diffusion coefficient $D=\frac{1}{2}\tau v_F^2$, and the result of Eq. (2c) suggests that in p-doped TMDCs spin-diffusion lengths

$$L_{is}^{(a)}=\sqrt{D\tau_{is}}\sim\sqrt{\hbar^3\tau/2\Theta_{is}m_*^3} \tag{3}$$

are almost independent of the carrier density at $n_h\to 0$.

The corrections due to quantum interference are exppressed in terms of particle-particle correlation functions known as cooperons, whose dynamics are governed by the Bethe-Salpeter equation, diagrammatically depicted in Fig. 2. Since spin and valley degrees of freedom are coupled in this regime, we simplify the notation by introducing a set of generators of U(2), $\sigma_{0,x,y,z}$, with σ_0 the identity and $\sigma_{x,y,z}$ Pauli matrices acting on the Hilbert space span by the doublet $(\mathbf{K}_+,\uparrow),(\mathbf{K}_-,\downarrow)$ [49]. First, we decompose the disorder correlators introduced in the main text [Fig. 2(a)] and cooperons [Fig. 2(b)] in singlet

TABLE II. Effective mass, SO splitting, and mobilities for conduction (e^-) and valence (h^+) bands of some best-studies semiconducting TMDCs.

Material	Band	$\frac{m^*}{m_0}$	λ (meV)	Mobility (cm^2/sV)
MoS_2	e^-	0.46 [25,42]	3 [25,42]	20–350 [7,11,15–18]
	h^+	0.54 [25,42]	148 [25,42]	
$MoSe_2$	e^-	0.56 [42]	22 [42]	
	h^+	−0.59 [42]	186 [42]	
WS_2	e^-	0.26 [42]	−32 [42]	
	h^+	−0.35 [42]	430 [19,22,42]	50–120 [20]
WSe_2	e^-	0.28 [42]	−37 [42]	
	h^+	−0.36 [42]	460 [19,22,42]	140 [10]

$(l,s=0)$ and triplet $(l,s=x,y,z)$ modes as

$$C_{ss'} \equiv \tfrac{1}{2}[\sigma_y\sigma_s]_{\alpha\beta}C_{\alpha\beta\alpha'\beta'}[\sigma_{s'}\sigma_y]_{\beta'\alpha'},$$
$$W_{ss'} \equiv \tfrac{1}{2}[\sigma_y\sigma_s]_{\alpha\beta}W_{\alpha\beta\alpha'\beta'}[\sigma_{s'}\sigma_y]_{\beta'\alpha'},$$

where the sum in $\alpha,\beta,\alpha',\beta'$ indices is assumed. Then, the Bethe-Salpeter equations [Fig. 2(c)] can be written in a compact way as

$$C_{s_1s_2}(\mathbf{Q},\omega) = W_{s_1s_2} + \sum_{s,s'}\sum_{l,l'} W_{s_1s'}C_{ss_2}(\mathbf{Q},\omega)\,\Pi_{ss'}(\mathbf{Q},\omega),$$

where

$$\Pi_{ss'}(\mathbf{Q},\omega) \equiv \frac{1}{2}\int\frac{d^2\mathbf{p}}{(2\pi\hbar)^2}\mathrm{Tr}[\sigma_s\sigma_y(\hat{G}^R(\mathbf{p},\hbar\omega+\varepsilon_F))^T \times \sigma_y\sigma_{s'}\hat{G}^A(\mathbf{Q}-\mathbf{p},\varepsilon_F)]. \quad (4)$$

The retarded/advanced Green operators are just

$$\hat{G}^{R,A}(\mathbf{p},\omega) = \frac{1}{\hbar\omega-\varepsilon_{\mathbf{p}}\pm i\frac{\hbar}{2\tau}}\sigma_0, \quad (5)$$

so then we have

$$\Pi_{ss'}(\mathbf{Q},\omega) = \approx\frac{2\pi\nu\tau}{\hbar}(1+i\tau\omega-\tau D|\mathbf{Q}|^2)\times\delta_{ss'}, \quad (6)$$

where the last result corresponds to the polarization operator in the so-called *diffusive approximation* $(\tau D\,|\mathbf{Q}|^2,\tau\omega\ll 1)$.

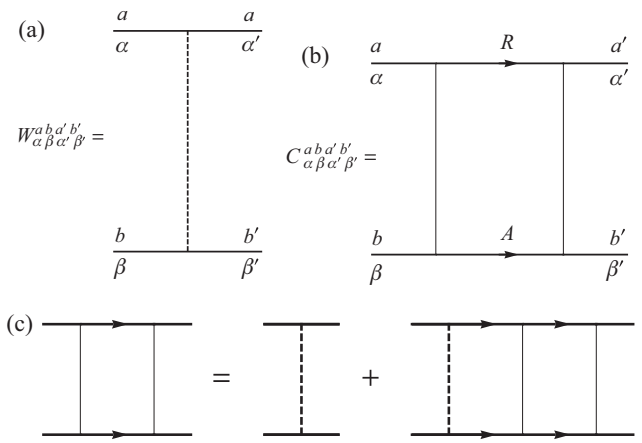

FIG. 2. Diagrammatic representation of (a) disorder correlator, (b) cooperon, and (c) Bethe-Salpeter equation.

The WL correction to conductivity can be written as the contribution of four cooperon modes [one singlet $s=0$ and three triplet $s=x,y,z$, with $\tilde{C}_s \equiv \frac{2\pi\nu\tau^2}{\hbar}C_{ss}(\mathbf{Q})$]

$$\delta g_{ii} = -\frac{2e^2D}{\pi\hbar}\int\frac{d^2\mathbf{Q}}{(2\pi)^2}[\tilde{C}_x+\tilde{C}_y+\tilde{C}_z-\tilde{C}_0], \quad (7)$$

which are fundamental solutions of diffusion-relaxation kernels

$$[-D\nabla^2 - i\omega+\Gamma_s]\tilde{C}_s(\mathbf{r}-\mathbf{r}',\omega) = \delta(\mathbf{r}-\mathbf{r}'). \quad (8)$$

This is deduced from the Bethe-Salpeter equation (4), assuming the low frequency and momentum expansion for the polarization operator (6), and also that diagonal scattering dominates over the rest, $\tau/\tau_0\sim 1$ [50].

The relations between the relaxation gaps Γ_s and the rates associated to different scattering mechanisms are summarized in Table III. Similarly to other multivalley conductors without intervalley scattering, lattice defects [34–37,48] and trigonal warping in the valley dispersion [36,37] suppress the low-temperature part of the quantum correction to conductivity caused by the interference of phase-coherent diffusive waves encircling the same random walk trajectory in the reversed directions. This is because inhomogeneous deformations generate a random pseudomagnetic field with the opposite sign in $K_\pm$ valleys, whereas trigonal anisotropy splits hole's wave number for the opposite Fermi velocity directions, hence inducing a random phase difference for the clockwise and anticlockwise propagating waves (Fig. 3) (with the opposite sign in the opposite valleys). The cumulative effect of these two factors determines the decay rate τ_*^{-1} of valley-polarized cooperons [36,37,48] in the set of triplet and singlet two-hole correlation functions

$$\tau_*^{-1} = 2\tau_g^{-1} + \frac{15\mu^2p_F^6\tau}{4\hbar^2} \propto An_h + Cn_h^3. \quad (9)$$

TABLE III. Relation between cooperon relaxation gaps and scattering rates in the regime A.

Relaxation gaps	Relaxation rates
$\Gamma_0 = 0$	$\tau^{-1} = \tau_0^{-1}+\tau_g^{-1}++\tau_{is}^{-1}$
$\Gamma_x = \Gamma_y = \tau_*^{-1}+\tau_{is}^{-1}$	
$\Gamma_z = 2\tau_{is}^{-1}$	$\tau_*^{-1} = 2\tau_g^{-1}+\frac{15\mu^2p_F^6\tau}{4\hbar^2}$

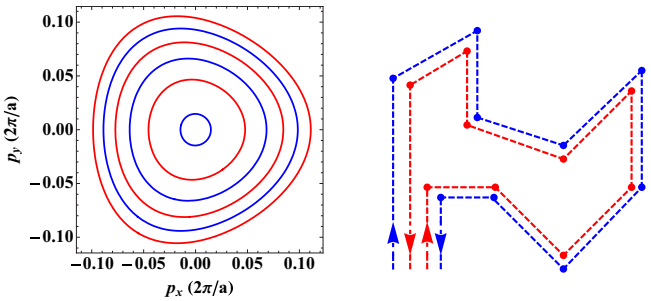

FIG. 3. (Color online) Trigonal warping of isoenergy contours in the valence band in one of the valleys (left), leading to a phase difference between holes propagating along a closed path in the reverse directions (right).

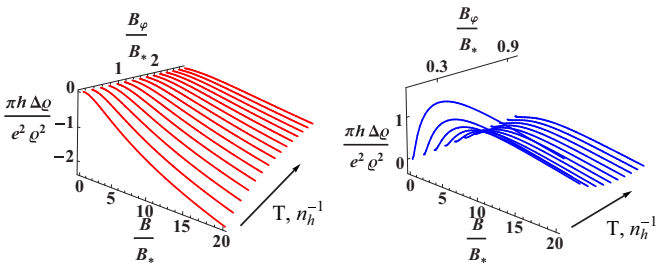

FIG. 4. (Color online) MR behavior in regime A as a function of applied magnetic field B and phase-coherence lengths through $B_\varphi \propto \ell_\varphi^{-2}$. Left (in red): no intervalley scattering, $\tau_{is} \to \infty$. WL saturates at temperatures/hole densities such that $\tau_\varphi \sim \tau_*$. Right (in blue): intervalley scattering is present, $\tau_{is} \sim \tau_*$. MR displays a crossover from WL to WAL upon increasing hole densities (decreasing B_φ).

Note that, similarly to L_{is} in Eq. (3),

$$L_* \equiv \sqrt{D\tau_*} \sim \sqrt{\hbar^3\tau/(\Theta_g + \Theta_{gz})m_*^3} \tag{10}$$

is independent of hole densities at $n_h \to 0$.

In the diffusive approximation, the integration in Eq. (7) has a natural ultraviolet cutoff imposed by the inverse of the mean-free path $\ell = \sqrt{D\tau}$, whereas the infrared cutoff is imposed by the decoherence length $\ell_\varphi = \sqrt{D\tau_\varphi}$. Then, the WL correction to conductivity reads just as

$$\delta g = \frac{e^2}{\pi h}\left[\ln\left(\frac{\tau^{-1}}{\tau_\varphi^{-1}}\right) - \ln\left(\frac{\tau^{-1}}{\tau_\varphi^{-1} + 2\tau_{is}^{-1}}\right) - 2\ln\left(\frac{\tau^{-1}}{\tau_\varphi^{-1} + \tau_{is}^{-1} + \tau_*^{-1}}\right)\right]. \tag{11}$$

In the presence of an out-of-plane magnetic field B, $|\mathbf{Q}|^2$ is quantized into $Q_n^2 = (n + 1/2)\,\ell_{B_z}^{-2}$, with the magnetic length defined as $\ell_B = \sqrt{\hbar/4eB}$. For $\ell_B \gg \ell$ the diffusive approximation is still valid, and the WL correction to conductivity reads as

$$\delta g_{ii}(B) = -\frac{e^2 D\ell_B^{-2}}{\pi h}\sum_s\sum_{n=0}^{n_{\max}}\frac{c_s}{D\ell_B^{-2}\left(n+\frac{1}{2}\right) + \Gamma_s + \tau_\varphi^{-1}},$$

with $c_{0,x,y,z} = -1,+1,+1,+1$. Thanks to the property of the digamma function

$$\psi(x + n_{\max} + 1) - \psi(x) = \sum_{n=0}^{n_{\max}}\frac{1}{x+n},$$

we can perform the summation, leading to

$$\delta g_{ii}(B) = -\frac{e^2}{\pi h}\sum_s c_s\left[\ln\left(\frac{\hbar\tau^{-1}}{4eDB}\right) - \psi\left(\frac{1}{2} + \frac{B_s + B_\varphi}{B}\right)\right],$$

with $B_s = \frac{\hbar\Gamma_s}{4eD}$. Note that we have taken the limit $n_{\max} \to \infty$,

$$\psi\left(x + n_{\max} + \frac{3}{2}\right) \to \ln(n_{\max}) \approx \ln\left(\frac{\hbar\tau^{-1}}{4eDB}\right).$$

Substrating the zero-field correction, the MR defined as $\Delta\rho(B) = \rho(B) - \rho(0) = -\Delta g(B)/\rho^2$ can be written as

$$\frac{\Delta\rho(B)}{\rho^2} = \frac{e^2}{\pi h}\left[F\left(\frac{B}{B_\varphi}\right) - F\left(\frac{B}{B_\varphi + 2B_{is}}\right) - 2F\left(\frac{B}{B_\varphi + B_{is} + B_*}\right)\right], \tag{12}$$

$$F(z) \equiv \ln(z) + \psi\left(\frac{1}{2} + \frac{1}{z}\right), \quad B_\alpha \equiv \frac{\hbar/e}{4D\tau_\alpha}.$$

Without intervalley scattering, the combined effect of pseudomagnetic disorder and trigonal warping places the system in the double-unitary symmetry class [31,51] with a WL peak saturated at a temperature such that $\tau_\varphi(T) \sim \tau_*$, and this interplays with spin-flip intervalley scattering which drives the system to the WAL regime. The resulting behavior of MR is illustrated in Fig. 4. From the density dependence of relaxation rates τ_{is}^{-1} and τ_*^{-1}, $B_{is} \propto L_{is}^{-2}$ and $B_* \propto L_*^{-2}$ should be finite at $n_h \to 0$ [see Eqs. (3) and (10)], in contrast to $B_\varphi \propto n_h^{-1}$. Hence, we conclude that magnetoresistance displays a crossover from WL to WAL behavior upon increasing the hole density. Here, the form of MR would be dependent on the amount of atomic defects responsible for the spin-flip intervalley scattering: for a virtually defectless crystal, MR would display a two-step crossover, from suppressed WL to WAL (this behavior is exactly the reverse of the WAL-WL crossover in monolayer graphene [36]).

B. Regime B: $\varepsilon_F \gtrsim \lambda$ (valence band)

When some minority-spin carriers are present on top of majority-spin Fermi seas in both valleys, both intravalley spin-flip and intervalley spin-conserving scattering are permitted for carriers at the Fermi level. Those are characterized by the intervalley τ_v^{-1} and spin-flip intravalley τ_{sf}^{-1} scattering rates

$$\tau_{v/sf}^{-1} = \frac{4\pi\nu}{\hbar}\left[\Upsilon_{v/sf} + p_F^2\,\Xi_{v/sf}\right], \tag{13}$$

parametrized by the correlation functions

$$\left\langle u_{sf}^i(\mathbf{r})u_{sf}^j(\mathbf{r}')\right\rangle = \Upsilon_{sf}\delta_{ij}\delta(\mathbf{r}-\mathbf{r}'),$$
$$\left\langle w_\alpha^i(\mathbf{r})w_\beta^j(\mathbf{r}')\right\rangle = \Xi_{sf}\delta_{\alpha\beta}\delta_{ij}\delta(\mathbf{r}-\mathbf{r}'),$$
$$\left\langle u_i^i(\mathbf{r})u_i^j(\mathbf{r}')\right\rangle = \Upsilon_v\delta_{ij}\delta(\mathbf{r}-\mathbf{r}'),$$
$$\left\langle w_{z\alpha}^i(\mathbf{r})w_{z\beta}^j(\mathbf{r}')\right\rangle = \Xi_v\delta_{\alpha\beta}\delta_{ij}\delta(\mathbf{r}-\mathbf{r}').$$

In the crystals with short-range (atomic) defects, these rates are independent of the carrier density, whereas in a clean smoothly bent layer they would linearly increase with the density of carriers.

Firing up new scattering processes at the carrier density threshold $n_c = n_h(\varepsilon_F = \lambda)$ reduces both the mean-free path of carriers and their spin-diffusion length (now, limited by the intravalley spin flip). The reduction of the mean-free path by additional scattering channels leads to a step change in the resistivity and spin relaxation upon the increase of the density across the threshold,

$$\rho(n_h) \approx \rho(n_c) + \frac{m}{e^2 n_h}\left(\tau_v^{-1} + \tau_{sf}^{-1}\right)\theta(n_h - n_c), \qquad (14)$$

followed by a gradual decrease of resistivity, with a slope determined by the mobilities of majority- and minority-spin carriers.

An abrupt change also occurs in the behavior of the quantum correction to conductivity of defected TMDCs. In short, opening intervalley and spin-flip intravalley scattering channel, with finite rates already at $n_h \geqslant n_c$, drives the system deeper into the symplectic symmetry class. This statement is based on the diagrammatic calculation, where now, similarly to graphene [52], one can classify cooperons as singlets and triplets in terms of both spin (s) and valley (l) indexes

$$C_{ss'}^{ll'} \equiv \tfrac{1}{4}[s_y s_s]_{\alpha\beta}[\tau_x \tau_l]^{ab} C_{\alpha\beta\alpha'\beta'}^{aba'b'}[s_{s'} s_y]_{\beta'\alpha'}[\tau_{l'}\tau_x]^{b'a'}.$$

The Bethe-Salpeter equations for the cooperons can be written in a compact way as

$$C_{s_1 s_2}^{l_1 l_2}(\mathbf{Q},\omega) = W_{s_1 s_2}^{l_1 l_2} + \sum_{s,s'}\sum_{l,l'} W_{s_1 s'}^{l_1 l'} C_{s s_2}^{l l_2}(\mathbf{Q},\omega)\,\Pi_{ss'}^{ll'}(\mathbf{Q},\omega),$$

where now the polarization operator reads as

$$\Pi_{ss'}^{ll'}(\mathbf{Q},\omega) \equiv \frac{1}{4}\int \frac{d^2\mathbf{p}}{(2\pi\hbar)^2}\mathrm{Tr}[(\tau_l\tau_x)\otimes(s_s s_y)(\hat{G}^R(\mathbf{p},\hbar\omega+\varepsilon_F))^T \times (\tau_x\tau_{l'})\otimes(s_y s_{s'})\hat{G}^A(\mathbf{Q}-\mathbf{p},\varepsilon_F)], \qquad (15)$$

and the disorder-averaged Green operators are

$$\hat{G}^{R,A}(\mathbf{p},\omega) = \frac{\left(\hbar\omega - \varepsilon_{\mathbf{p}} \pm i\frac{\hbar}{2\tau}\right) + \frac{\lambda}{2}\tau_z\otimes s_z}{\left(\hbar\omega - \varepsilon_{\mathbf{p}} \pm i\frac{\hbar}{2\tau}\right)^2 - \frac{\lambda^2}{4}}. \qquad (16)$$

Hence, the WL correction to conductivity is given by 16 cooperon modes ($\tilde{C}_s^l \equiv \frac{2\pi\nu\tau^2}{\hbar} C_{ss}^{ll}$)

$$\delta g_{ii} = -\frac{2e^2 D}{\pi\hbar}\int\frac{d^2\mathbf{Q}}{(2\pi)^2}\sum_{s,l} c_s c^l \tilde{C}_s^l(\mathbf{Q}), \text{ with}$$
$$c_{0,x,y,z} = -1,+1,+1,+1, \qquad (17)$$
$$c^{0,x,y,z} = +1,+1,+1,-1.$$

As before, we take the low momentum and frequency expansion of the polarization operator assuming the diffusive approximation $\tau D|\mathbf{Q}|^2, \tau\omega \ll 1$. Two groups of four cooperons corresponding to singlet and triplet combinations built separately of two Kramers doublets $(K_+,\uparrow; K_-,\downarrow)$ and $(K_+,\downarrow; K_-,\uparrow)$ are solutions of the diffusion-relaxation kernels

$$\left[-D\nabla^2 - i\omega + \Gamma_s^l\right]\tilde{C}_s^l(\mathbf{r}-\mathbf{r}',\omega) = \delta(\mathbf{r}-\mathbf{r}'), \qquad (18)$$

whereas the cross-doublet cooperons do not contribute in the present regime due to the mismatch between the Fermi surfaces corresponding to different spin polarizations at each valley. The WL correction to conductivity and MR in this regime reads as, in general,

$$\delta g = \frac{e^2}{\pi h}\left[\ln\left(\frac{\tau^{-1}}{\tau_\varphi^{-1}}\right) + \ln\left(\frac{\tau^{-1}}{\tau_\varphi^{-1}+\Gamma_z^z}\right) - \ln\left(\frac{\tau^{-1}}{\tau_\varphi^{-1}+\Gamma_z^0}\right) - \ln\left(\frac{\tau^{-1}}{\tau_\varphi^{-1}+\Gamma_0^z}\right) - 4\ln\left(\frac{\tau^{-1}}{\tau_\varphi^{-1}+\Gamma_x^x}\right)\right],$$
$$\frac{\Delta\rho(B)}{\rho^2} = \frac{e^2}{\pi h}\left[F\left(\frac{B}{B_\varphi}\right) + F\left(\frac{B}{B_\varphi+B_z^z}\right) - F\left(\frac{B}{B_\varphi+B_z^0}\right) - F\left(\frac{B}{B_\varphi+B_0^z}\right) - 4F\left(\frac{B}{B_\varphi+B_x^x}\right)\right], \qquad (19)$$

where the expressions for the relaxation gaps are summarized in Table IV and we have introduced $B_s^l = \frac{\hbar\Gamma_s^l}{4eD}$.

These expressions can be further simplified if we neglect τ_*^{-1} and τ_{is}^{-1} in the expression for Γ_x^x, Γ_0^z, and Γ_z^0, which are assumed to be smaller due to their dependence on carrier concentration. Then, we have

$$\delta g = \frac{e^2}{\pi h}\left[\ln\frac{\left(\tau_\varphi^{-1}+2\tau_{sf}^{-1}\right)\left(\tau_\varphi^{-1}+2\tau_v^{-1}\right)}{\tau_\varphi^{-1}\left(\tau_\varphi^{-1}+2\tau_v^{-1}+2\tau_{sf}^{-1}\right)} - 4\ln\left(\frac{\tau^{-1}}{\tau_\varphi^{-1}+\tau_v^{-1}+\tau_{sf}^{-1}}\right)\right];$$
$$\frac{\Delta\rho(B)}{\rho^2} = \frac{e^2}{\pi h}F\left(\frac{B}{B_\varphi}\right) - \frac{e^2}{96\pi h}\left[\frac{15B^2}{(B_v+B_{sf})^2} + \frac{B^2}{B_v^2} + \frac{B^2}{B_{sf}^2}\right], \qquad (20)$$

where we have expanded all the $F(z)$ functions to the lowest order excepting the first term and $B_\alpha = \hbar/(4e\tau_\alpha D)$. Note that in this regime, intravalley spin-flip processes do not lead immediately to WAL. This happens because the fourth term in the first line of Eq. (1b) looks like intravalley magnetic disorder which suppresses WAL effect coming from intravalley

TABLE IV. Relation between cooperon relaxation gaps and scattering rates in regimes B and C.

Relaxation gaps	Relaxation rates
$\Gamma_0^0 = 0$	$\tau^{-1} = \tau_0^{-1} + \tau_g^{-1} + \tau_v^{-1} + \tau_{sf}^{-1} + \tau_{is}^{-1}$
$\Gamma_x^0 = \Gamma_y^0 = \tau_\lambda^{-1} + 2\tau_{gz}^{-1} + \tau_v^{-1} - \tau_{\gamma_v}^{-1} + \tau_{sf}^{-1} + \tau_{is}^{-1}$	
$\Gamma_z^0 = 2\tau_{sf}^{-1} + 2\tau_{is}^{-1}$	$\tau_{gz}^{-1} = \frac{2\pi\nu p_F^2 \Theta_{gz}}{\hbar}$
$\Gamma_0^x = \Gamma_0^y = \tau_\lambda^{-1} + \tau_{**}^{-1} + \tau_{sf}^{-1} + \tau_{\gamma_{sf}}^{-1} + \tau_v^{-1} + \tau_{is}^{-1}$	
$\Gamma_x^x = \Gamma_x^y = \Gamma_y^x = \Gamma_y^y = \tau_*^{-1} + \tau_v^{-1} + \tau_{sf}^{-1} + \tau_{is}^{-1}$	$\tau_{**}^{-1} = \tau_*^{-1} - 2\tau_{gz}^{-1}$
$\Gamma_z^x = \Gamma_z^y = \tau_\lambda^{-1} + \tau_{**}^{-1} + \tau_{sf}^{-1} - \tau_{\gamma_{sf}}^{-1} + \tau_v^{-1} + \tau_{is}^{-1}$	
$\Gamma_0^z = 2\tau_v^{-1} + 2\tau_{is}^{-1}$	$\tau_{\gamma_{sf}}^{-1} = \frac{4\pi\nu}{\hbar}\left[\Upsilon_{sf} - p_F^2 \Xi_{sf}\right]$
$\Gamma_x^z = \Gamma_y^z = \tau_\lambda^{-1} + 2\tau_{gz}^{-1} + \tau_v^{-1} - \tau_{\gamma_v}^{-1} + \tau_{sf}^{-1} + \tau_{is}^{-1}$	
$\Gamma_z^z = 2\tau_v^{-1} + 2\tau_{sf}^{-1}$	$\tau_{\gamma_v}^{-1} = \frac{4\pi\nu}{\hbar}\left[\Upsilon_v - p_F^2 \Xi_v\right]$

spin-flip scattering, similarly to how trigonal warping and Berry curvature [accounted by τ_*^{-1} in Eqs. (11) and (12)] suppress WL in the transport regime A.

C. Regime C: $\varepsilon_F \gg \lambda$ (conduction band)

In this case, the crossover between WL and WAL behavior of magnetoresistance takes the most complicated form, especially when $\lambda\tau < \hbar$, since one has to take into account all 16 cooperons built using valley-spin quartet $(K_+,\uparrow; K_-,\downarrow; K_+,\downarrow; K_-,\uparrow)$. The intrinsic SO splitting acts as an effective Zeeman coupling making the electron spin precess around the axis perpendicular to the crystal plane in the opposite direction for electrons in the opposite valleys. SO splitting and spin-dependent disorder determine the rate

$$\tau_\lambda^{-1} = \frac{\lambda^2\tau}{\hbar^2} + \frac{4\pi\nu\Omega_z}{\hbar}, \tag{21}$$

at which the eight cooperon modes that we neglected previously, $\tilde{C}_{x,y}^{0,z}$ and $\tilde{C}_{0,z}^{x,y}$, decay. The SO splitting also couples them by precession with the rate $\omega_\lambda \equiv \lambda/\hbar$, similarly to how real Zeeman coupling mixes singlet/triplet cooperon modes in a simple disordered metal [53]. These modes satisfy the matrix equations (for the former)

$$\begin{pmatrix} \Pi + \Gamma_x^{0(z)} & -\omega_\lambda \\ \omega_\lambda & \Pi + \Gamma_y^{z(0)} \end{pmatrix} \begin{pmatrix} \tilde{C}_{xx}^{00(zz)} & \tilde{C}_{xy}^{0z(z0)} \\ \tilde{C}_{yx}^{z0(0z)} & \tilde{C}_{yy}^{zz(00)} \end{pmatrix} = \mathcal{I}, \tag{22}$$

where we have written $\Pi = D\,|\mathbf{Q}|^2 - i\omega$ for simplicity. After matrix inversion, we have

$$\begin{aligned} \tilde{C}_x^{0(z)} &= \frac{\Pi + \Gamma_y^{z(0)}}{\left(\Pi + \Gamma_x^{0(z)}\right)\left(\Pi + \Gamma_y^{z(0)}\right) + \omega_\lambda^2}, \\ \tilde{C}_y^{z(0)} &= \frac{\Pi + \Gamma_x^{0(z)}}{\left(\Pi + \Gamma_y^{z(0)}\right)\left(\Pi + \Gamma_x^{0(z)}\right) + \omega_\lambda^2}. \end{aligned} \tag{23}$$

For $\tilde{C}_{0,z}^{x,y}$ we obtain the same swapping the spin and valley indices. Then, by introducing the coefficients

$$\gamma_v \equiv \frac{\tau_{\gamma_v}^{-1}}{\sqrt{\tau_{\gamma_v}^{-2} - \omega_\lambda^2}}, \quad \gamma_{sf} \equiv \frac{\tau_{\gamma_{sf}}^{-1}}{\sqrt{\tau_{\gamma_{sf}}^{-2} - \omega_\lambda^2}},$$

where the rates $\tau_{\gamma_v}^{-1}$, $\tau_{\gamma_{sf}}^{-1}$ are defined in the second column of Table IV, the WL correction to conductivity and MR can be written as

$$\begin{aligned} \delta g = \frac{e^2}{\pi h}\Bigg\{ & \ln\left(\frac{\tau^{-1}}{\tau_\varphi^{-1}}\right) + \ln\left(\frac{\tau^{-1}}{\tau_\varphi^{-1} + \Gamma_z^z}\right) - \ln\left(\frac{\tau^{-1}}{\tau_\varphi^{-1} + \Gamma_z^0}\right) - \ln\left(\frac{\tau^{-1}}{\tau_\varphi^{-1} + \Gamma_0^z}\right) - 4\ln\left(\frac{\tau^{-1}}{\tau_\varphi^{-1} + \Gamma_x^x}\right) \\ & + 2\gamma_v\left[\ln\left(\frac{\tau_{\gamma_v}^{-1} + \tau^{-1}\gamma_v}{\tau_{\gamma_v}^{-1} - \tau^{-1}\gamma_v}\right) - \ln\left(\frac{\tau_{\gamma_v}^{-1} + \left(\tau_\varphi^{-1} + \Gamma_x^0/2 + \Gamma_x^z/2\right)\gamma_v}{\tau_{\gamma_v}^{-1} - \left(\tau_\varphi^{-1} + \Gamma_x^0/2 + \Gamma_x^z/2\right)\gamma_v}\right)\right] \\ & + 2\gamma_{sf}\left[\ln\left(\frac{\tau_{\gamma_{sf}}^{-1} + \tau^{-1}\gamma_s}{\tau_{\gamma_{sf}}^{-1} - \tau^{-1}\gamma_s}\right) - \ln\left(\frac{\tau_{\gamma_{sf}}^{-1} + \left(\tau_\varphi^{-1} + \Gamma_0^x/2 + \Gamma_z^x/2\right)\gamma_s}{\tau_{\gamma_{sf}}^{-1} - \left(\tau_\varphi^{-1} + \Gamma_0^z/2 + \Gamma_z^x/2\right)\gamma_s}\right)\right]\Bigg\}, \\ \frac{\Delta\rho\,(B)}{\rho^2} = \frac{e^2}{\pi h}\Bigg[& F\left(\frac{B}{B_\varphi}\right) + F\left(\frac{B}{B_\varphi + B_z^z}\right) - F\left(\frac{B}{B_\varphi + B_z^0}\right) - F\left(\frac{B}{B_\varphi + B_0^z}\right) - 4F\left(\frac{B}{B_\varphi + B_x^x}\right) \\ & + 2\gamma_v G\left(\frac{B}{B_\varphi + \frac{B_x^0 + B_x^z}{2}}, \frac{\gamma_v B}{B_{\gamma_v}}\right) + 2\gamma_{sf} G\left(\frac{B}{B_\varphi + \frac{B_0^x + B_z^x}{2}}, \frac{\gamma_{sf} B}{B_{\gamma_{sf}}}\right)\Bigg], \end{aligned} \tag{24}$$

where $B_{\gamma_{v,sf}} \equiv \frac{\hbar}{4eD\tau_{\gamma_{v,sf}}}$, and

$$G(z_1,z_2) \equiv \sum_{\pm}\left[\pm\psi\left(\frac{1}{2}+\frac{1}{z_1}\pm\frac{1}{z_2}\right)\mp\ln\left(\frac{1}{z_1}\pm\frac{1}{z_2}\right)\right].$$

We analyze the quantum transport behavior in TMDCs deduced from these formulas in two extreme situations depending on their crystalline quality: (i) material where scattering is dominated by lattice defects and (ii) defect-free TMDC.

1. Lattice-disordered TMDCs

We take into account only such disorder that leads to finite scattering rates $\tau_{0,v,sf}^{-1}$ for electrons at the edge of conduction band, leading to

$$\gamma_{v,sf} = \frac{1}{\sqrt{1-\frac{\lambda^2\tau_{v,sf}^2}{\hbar^2}}}.$$

In this case, MR has a distinct WAL form, extrapolated from the WAL behavior in the regime B:

$$\frac{\Delta\rho(B)}{\rho^2} = \frac{e^2}{\pi h}F\left(\frac{B}{B_\varphi}\right) - \frac{e^2}{96\pi h}\left[\frac{15B^2}{(B_v+B_{sf})^2}+\frac{B^2}{B_v^2}+\frac{B^2}{B_{sf}^2} + \sum_{\alpha=v,sf}\frac{32B_\alpha(B_\lambda+B_v+B_{sf})B^2}{\left[\tilde{B}_\lambda^2+(B_\lambda+B_{sf}+B_v)^2-B_\alpha^2\right]^2}\right], \quad (25)$$

where we have expanded $F(z)$ and $G(z)$ to the lowest order in z and $B_\alpha = \hbar/(4e\tau_\alpha D)$, $\tilde{B}_\lambda = \lambda/(4eD)$.

2. TMDCs free of atomic defects

In a defect-free 2D crystal with scattering produced by remote charges in the substrate or smooth lattice deformations, electrons diffuse conserving their valley state ($\tau_{v,is}\to\infty$). Then, spin-diffusion lengths

$$L_s^{(c)} \sim \frac{\hbar p_F}{\lambda m_*}\times\max\left[\frac{\mathcal{L}}{\sqrt{2\langle h^2\rangle}},\sqrt{\frac{2\pi\kappa}{K_BT}}\right]\propto\sqrt{n_e} \quad (26)$$

are assumed to be limited by either the characteristic height $\sqrt{\langle h^2\rangle}$ of static wrinkles of lateral size $\mathcal{L}$, or temperature in the case of flexural vibration modes, where κ is bending stiffness of the 2D crystal [43,54].

As to the quantum transport, spurious time-inversion asymmetry for the intravalley electron propagation caused by SO coupling, Berry phase, and pseudomagnetic field due to the deformations suppress the interference correction to conductivity. As a result, MR in such high-quality 2D material would have a form of a suppressed WL effect

$$\frac{\Delta\rho(B)}{\rho^2} = -\frac{2e^2}{\pi h}\left\{2F\left(\frac{B}{B_\varphi+B_{sf}}\right)+\frac{1}{\sqrt{1-\frac{\lambda^2\tau_{sf}^2}{\hbar^2}}}\times G\left(\frac{B}{B_\varphi+B_\lambda+B_{sf}},\frac{B}{B_{sf}\sqrt{1-\frac{\lambda^2\tau_{sf}^2}{\hbar^2}}}\right)\right\}. \quad (27)$$

IV. DISCUSSION

For n-doped TMDCs (regime C), it is interesting to discuss the extreme of samples free of atomic defects, where the expression for the MR adopts its easiest form (27). We see that the suppression of WL is governed by the ratio between the spin-relaxation rate τ_{sf}^{-1} and the characteristic precession frequency defined by the SO splitting ω_λ. Taking MoS_2 as a reference, we have $\tau_{sf}\sim 1$ ns [43,54], which is compatible with optical experiments [55], whereas the precession frequencies are of the order of THzs, leading to $\tau_{sf}\omega_\lambda\sim 10^3$. Thus, WL behavior is expected, eventually suppressed by warping or Berry phase effects. Hence, if an experiment on n-doped MoS_2 displayed WAL behavior, this would immediately point at the presence of short-range disorder (such as vacancies in the chalcogen atoms layer, which break the $z\to -z$ symmetry of the system) which scatters between valleys simultaneously flipping spins.

For p-doped TMDCs, spin relaxation has a rate linear in the carrier density for $\varepsilon_F(n_h)<\lambda$, which leads to a density-independent spin-diffusion length, and that their MR displays a crossover from WL to WAL behavior upon the increase in the concentration of holes. At the threshold density n_c of the population of minority-spin states in each valley $\varepsilon_F(n_c)=\lambda$, resistivity and spin relaxation rate of holes undergo a steplike increase, whereas the quantum correction to conductivity remains of a WAL type.

To complete this discussion, we also consider a generally ignored but possible occurrence of the Γ-point band edge in some TMDCs. To the lowest orders in momentum, the $\mathbf{k}\cdot\mathbf{p}$ Hamiltonian, including SO terms, reads as

$$\mathcal{H} = \frac{|\mathbf{p}|^2}{2m^*}+\alpha\left(p_x^3-3p_xp_y^2\right)s_z. \quad (28)$$

The SO parameter can be roughly estimated as $\alpha\approx\lambda/(\hbar^3|K_\pm|^3)=(\frac{\sqrt{3}a}{4\pi\hbar})^3\lambda$. For a finite concentration of holes around Γ, n_Γ, we have

$$\frac{\alpha p_F^3}{\hbar/\tau}\sim\ell a^3n_c^2\left(\frac{n_\Gamma}{n_c}\right)^{\frac{3}{2}}\ll 1.$$

Hence, the spin splitting of electron states near the Γ point plays no role, whereas $z\to -z$ symmetry-breaking flexural deformations and substrate-induced asymmetry would lead to the typical Bychkov-Rashba SO effects [56], Dyakonov-Perel [57,58] spin relaxation, and WL-WAL crossover, as in GaAs/AlGaAs heterostructures [51,59,60]. This should be contrasted with suppressed WL behavior in high-quality, low-to-medium p-doped samples characteristic for $K_\pm$ points band edges. With the references to Eqs. (11) and (12), we suggest

that if fitting of experimentally measured magnetoresistance returned τ_* such that $\tau \ll \tau_* \ll \tau_\varphi$, this would give a distinct quantitative proof for the multivalley nature of the valence band edge.

ACKNOWLEDGMENTS

The authors thank I. Aleiner and A. Morpurgo for useful discussions. This work was supported by CSIC JAE-Pre Grant, EC FP7 Graphene Flagship Project No. CNECT-ICT-604391, ERC Synergy Grant Hetero2D, the Royal Society Wolfson Research Merit Award, Marie-Curie-ITN 607904-13 Spinograph, and ERC Advanced Grant No. 290846.

APPENDIX A: $\mathbf{k}\cdot\mathbf{p}$ THEORY FOR ELECTRONS AND HOLES IN TMDCS

In this Appendix, we deduce the band Hamiltonian of Eq. (1a) from a $\mathbf{k}\cdot\mathbf{p}$ theory describing lowest conduction and valence bands [22,25]. These are dominated by d orbitals from the M atoms $d_{3z^2-r^2}$ and $(d_{x^2-y^2} \pm i d_{xy})$, respectively. Instead of dealing with degenerate states at $\mathbf{K}_\pm$ points one can triple the unit cell in such a way that the old $K_\pm$ points are now equivalent to the Γ point of the folded Brillouin zone. From the point of view of the lattice symmetries, this means that the two elementary translations $(\mathbf{t}_{\mathbf{a}_1}, \mathbf{t}_{\mathbf{a}_2})$ are factorized out of the translation group and added to the point group D_{3h}, which becomes $D''_{3h} = D_{3h} + \mathbf{t}_{\mathbf{a}_1} \times D_{3h} + \mathbf{t}_{\mathbf{a}_2} \times D_{3h}$. The character table of this group is shown in Table V. D''_{3h} contains 24 new elements and 6 additional conjugacy classes, which leads to 6 new two-dimensional irreducible representations (denoted by $E'_{1,2,3}$ and $E''_{1,2,3}$), the valley off-diagonal representations.

The symmetry properties of Bloch wave functions at the Brillouin zone corners are summarized in Table VI, which gives the suitable combination of atomic orbitals and the associated irreducible representation of D''_{3h}. In the case of X atoms, both bonding (b) and antibonding (ab) combinations of orbitals from the bottom and top layers are considered. The second and third columns contain the phases picked up by the wave function at each valley when a $2\pi/3$ rotation or a mirror reflection is performed. We consider the space of 4-vectors $\sim(E'_2, E'_1)$ whose entries represent the projection of the Bloch wave function at conduction and valence states at the Brillouin zone corners. In order to construct the effective $\mathbf{k}\cdot\mathbf{p}$ Hamiltonian acting on this subspace, we must consider the possible 16 Hermitian operators, whose reduction in terms of irreducible representations of D''_{3h} is inferred from

$$\left(E'_2, E'_1\right) \times \left(E'_2, E'_1\right) \sim 2A'_1 + 2A'_2 + 2E' + E'_1 + E'_2 + 2E'_3.$$

This space of electronic operators can be constructed from two commutating Pauli algebras Σ_i, Λ_i. The definitions are summarized in Table VII. The basis is $(\psi_{c+}, \psi_{v+}, \psi_{v-}, -\psi_{c-})$, where $\psi_{c,v\pm}$ represents the wave function of the conduction or valence state at $K_\pm$ points, in such a way that time-reversal operation (including spin) reads as $i s_y \Lambda_y \Sigma_y \mathcal{K}$. The operators Λ_i, Σ_i and all their combinations are 4×4 matrices, which in this basis can be written as

$$\Sigma_{x,y,z} = \tau_0 \otimes \sigma_{x,y,z},$$
$$\Lambda_{x,y,z} = \tau_{x,y,z} \otimes \sigma_0,$$

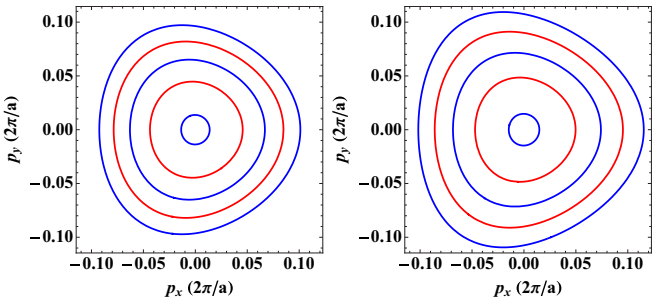

FIG. 5. (Color online) Isoenergy contours around $K_\pm$ points deduced from Eq. (A1) for conduction (left) and valence (right) bands. We take $\gamma = 3.82\,\mathrm{eV\,A}$, $\alpha = 1.72\,\mathrm{eV\,A^2}$, $\beta = -0.13\,\mathrm{eV\,A^2}$, and $\kappa = -1.02\,\mathrm{eV\,A^2}$ [25]. The spin-orbit splitting is neglected.

where τ_i and σ_i are Pauli matrices that act in valley and conduction/valence subspaces.

The Hamiltonian up to second order in $\mathbf{p}$ reads as [61]

$$\mathcal{H} = \gamma \mathbf{p}\cdot\boldsymbol{\Sigma} + \frac{\Delta}{2}\Lambda_z\Sigma_z + \frac{\alpha+\beta}{2}\mathcal{I}|\mathbf{p}|^2 + \frac{\alpha-\beta}{2}\Lambda_z\Sigma_z|\mathbf{p}|^2 + \kappa\left[\left(p_x^2 - p_y^2\right)\Lambda_z\Sigma_x - 2p_x p_y \Lambda_z \Sigma_y\right], \tag{A1}$$

which corresponds to the Hamiltonian in Eqs. (2a)–(2d) of Ref. [25]. Microscopically, the linear term in $\mathbf{p}$ comes from the strong hybridization between conduction and valence band states away from $K_\pm$ points, both dominated by orbitals localized in the metal transition-metal atoms. Such hybridization is responsible for the nonzero Berry curvature of the bands [62]

$$\Omega^\tau_{c,v}(\mathbf{p}) \approx \mp \frac{2\tau\gamma^2[\Delta - (\alpha-\beta)|\mathbf{p}|^2]}{[(\Delta + (\alpha-\beta)^2|\mathbf{p}|^2) + 4\gamma^2|\mathbf{p}|^2]^{3/2}}. \tag{A2}$$

The different orbital composition of conduction and valence bands introduces certain electron-hole asymmetry, and it is also responsible for the distinct strengths of the intrinsic spin-orbit splitting of the bands. We also include trigonal warping effects in the bands through the last term of the Hamiltonian. The isoenergy contours around $K_\pm$ points deduced from this model are shown in Fig. 5.

We project the Hamiltonian of Eq. (A1) onto a single band by a Schrieffer-Wolf transformation [63]. The Hamiltonian can be written in the block form as

$$\mathcal{H} = \begin{pmatrix} \mathcal{H}_c^{(0)} & V \\ V^\dagger & \mathcal{H}_v^{(0)} \end{pmatrix}. \tag{A3}$$

We take the Green's function $\mathcal{G} = (\epsilon - \mathcal{H})^{-1}$, then evaluate the block $\mathcal{G}_{c,v}$ associated to the conduction/valence band, and use it in order to identify the effective Hamiltonian near the band edge. If we define $\mathcal{G}^{(0)}_{c,v} = (\epsilon - \mathcal{H}^{(0)}_{c,v})^{-1}$, then we can write

$$\begin{pmatrix} \mathcal{G}_c & \mathcal{G}_{cv} \\ \mathcal{G}_{vc} & \mathcal{G}_v \end{pmatrix} = \begin{pmatrix} \left(\mathcal{G}_c^{(0)}\right)^{-1} & V \\ V^\dagger & \left(\mathcal{G}_v^{(0)}\right)^{-1} \end{pmatrix}^{-1}. \tag{A4}$$

For the conduction band, we obtain $\mathcal{G}_c = [(\mathcal{G}_c^{(0)})^{-1} - V\mathcal{G}_v^{(0)}V^\dagger]^{-1}$, so $\epsilon - \mathcal{G}_c^{-1} = \mathcal{H}_c + V\mathcal{G}_v^{(0)}V^\dagger$. At the bottom of the band ($\epsilon \approx \frac{\Delta}{2}$), the effective Hamiltonian to the lowest order

TABLE V. Character table of D''_{3h}.

D''_{3h}	E	$2T$	σ_h	$2T\sigma_h$	$2C_3$	$2TC_3$	$2TC_3^2$	$2S_3$	$2TS_3$	$2TS_3^2$	$9TC'_2$	$9T\sigma_v$
A'_1	1	1	1	1	1	1	1	1	1	1	1	1
A'_2	1	1	1	1	1	1	1	1	1	1	–1	–1
A''_1	1	1	–1	–1	1	1	1	–1	–1	–1	1	–1
A''_2	1	1	–1	–1	1	1	1	–1	–1	–1	–1	1
E'	2	2	2	2	–1	–1	–1	–1	–1	–1	0	0
E''	2	2	–2	–2	–1	–1	–1	1	1	1	0	0
E'_1	2	–1	2	–1	2	–1	–1	2	–1	–1	0	0
E''_1	2	–1	–2	1	2	–1	–1	–2	1	1	0	0
E'_2	2	–1	2	–1	–1	2	–1	–1	2	–1	0	0
E''_2	2	–1	–2	1	–1	2	–1	1	–2	1	0	0
E'_3	2	–1	2	–1	–1	–1	2	–1	–1	2	0	0
E''_3	2	–1	–2	1	–1	–1	2	1	1	–2	0	0

in Δ^{-1} reads as

$$\mathcal{H}_c \approx \mathcal{H}_c^{(0)} + \frac{V \begin{pmatrix} 0 & 0 \\ 0 & 1 \end{pmatrix} V^\dagger}{\Delta}. \tag{A5}$$

Similarly, for the valence band we have

$$\mathcal{H}_v \approx \mathcal{H}_v^{(0)} - \frac{V^\dagger \begin{pmatrix} 1 & 0 \\ 0 & 0 \end{pmatrix} V}{\Delta}. \tag{A6}$$

By this procedure we obtain the Hamiltonian in Eq. (1a) with

$$\begin{aligned} m^*_{c,v} &= \frac{1}{2\left(\alpha, \beta \pm \frac{\gamma^2}{\Delta}\right)}, \\ \mu_{c,v} &= \pm \frac{2\gamma\kappa}{\Delta}. \end{aligned} \tag{A7}$$

APPENDIX B: k · p THEORY FOR INTRAVALLEY AND INTERVALLEY DISORDER

In this Appendix, we deduce the form of the disorder potentials included in Eq. (1b). Within the two-bands $\mathbf{k}\cdot\mathbf{p}$ theory, intravalley disorder enters as *scalar*, *mass*, and *gauge* like potentials,

$$\delta\mathcal{H}(\mathbf{r}) = U(\mathbf{r})\mathcal{I} + M(\mathbf{r})\Lambda_z\Sigma_z + \Lambda_z\boldsymbol{\Sigma}\cdot\mathbf{A}(\mathbf{r}). \tag{B1}$$

TABLE VI. Classification of the Bloch wave functions at $K_\pm$ according to the irreducible representations of D''_{3h}. The sign $\pm$ corresponds to combinations of orbitals at $K_\pm$ points, and $w = e^{i\frac{2\pi}{3}}$.

Irreps	C_3	σ_h	M atom	X atoms
E'_1	1	1	$\frac{1}{\sqrt{2}}(d_{x^2-y^2} \pm id_{xy})$, $\frac{1}{\sqrt{2}}(p_x \mp ip_y)$	$\frac{1}{\sqrt{2}}(p_x \pm ip_y)$ (b)
E''_1	1	-1	$\frac{1}{\sqrt{2}}(d_{xz} \mp id_{yz})$	$\frac{1}{\sqrt{2}}(p_x \pm ip_y)$ (ab)
E'_2	$w^{\pm1}$	1	$d_{3z^2-r^2}$, s	$\frac{1}{\sqrt{2}}(p_x \mp ip_y)$ (b)
E'_3	$w^{\mp1}$	1	$\frac{1}{\sqrt{2}}(d_{x^2-y^2} \mp id_{xy})$, $\frac{1}{\sqrt{2}}(p_x \pm ip_y)$	p_z (ab), s (b)
E''_2	$w^{\pm1}$	-1	p_z	$\frac{1}{\sqrt{2}}(p_x \mp ip_y)$ (ab)
E''_3	$w^{\mp1}$	-1	$\frac{1}{\sqrt{2}}(d_{xz} \pm id_{yz})$	p_z (b), s (ab)

When we project these terms onto a single band by the same procedure as before we obtain

$$\delta\mathcal{H}_{c,v} = U_{c,v}(\mathbf{r}) \pm \frac{\gamma}{\Delta}\{\mathbf{p}, \mathbf{A}(\mathbf{r})\}\tau_z, \tag{B2}$$

with $U_{c,v}(\mathbf{r}) = U(\mathbf{r}) \pm M(\mathbf{r}) + \frac{\gamma}{\Delta}[\nabla \times \mathbf{A}(\mathbf{r})]_z$. This corresponds to first and third terms of Eq. (1b) of the main text with

$$\begin{aligned} u_0(\mathbf{r}) &= U(\mathbf{r}) \pm M(\mathbf{r}) + \frac{\gamma}{\Delta}[\nabla \times \mathbf{A}(\mathbf{r})]_z, \\ \mathbf{a}_g(\mathbf{r}) &= \pm\frac{\gamma}{\Delta}\mathbf{A}(\mathbf{r}). \end{aligned} \tag{B3}$$

Intervalley disorder can be incorporated following the same procedure. Within the two-bands model we have in general

$$V^{\text{int}}(\mathbf{r}) = \sum_{n=x,y,z}\sum_{l=x,y} V_{nl}(\mathbf{r})\Sigma_n\Lambda_l. \tag{B4}$$

We can write the spin-dependent disorder potentials in the same fashion, distinguishing even and odd terms

TABLE VII. Definitions of the electronic operators in the two bands effective model at $K_\pm$ points.

Irrep	$t \to -t$ even	$t \to -t$ odd
A'_1	$\mathcal{I}$, $\Lambda_z\Sigma_z$, $\Lambda_z s_z$, $\Sigma_z s_z$	
A'_2		Σ_z, Λ_z, s_z
A''_1	$\Sigma_x s_x + \Sigma_y s_y$	
A''_2	$\Sigma_x s_y - \Sigma_y s_x$	
E'	$\begin{pmatrix}-\Lambda_z\Sigma_y \\ \Lambda_z\Sigma_x\end{pmatrix}$, $\begin{pmatrix}-s_z\Sigma_y \\ s_z\Sigma_x\end{pmatrix}$	$\begin{pmatrix}\Sigma_x \\ \Sigma_y\end{pmatrix}$
E''	$\begin{pmatrix}\Lambda_z s_x \\ \Lambda_z s_y\end{pmatrix}$, $\begin{pmatrix}\Sigma_z s_x \\ \Sigma_z s_y\end{pmatrix}$, $\begin{pmatrix}\Sigma_x s_y + \Sigma_y s_x \\ \Sigma_x s_x - \Sigma_y s_y\end{pmatrix}$	$\begin{pmatrix}-s_y \\ s_x\end{pmatrix}$
E'_1	$\begin{pmatrix}\Sigma_x\Lambda_x + \Sigma_y\Lambda_y \\ \Sigma_x\Lambda_y - \Sigma_y\Lambda_x\end{pmatrix}$	
E''_1	$\begin{pmatrix}\Lambda_x s_y - \Lambda_y s_x \\ \Lambda_x s_x + \Lambda_y s_y\end{pmatrix}$	
E'_2	$\begin{pmatrix}\Sigma_y\Lambda_y - \Sigma_x\Lambda_x \\ -\Sigma_x\Lambda_y - \Sigma_y\Lambda_x\end{pmatrix}$	
E''_2	$\begin{pmatrix}\Lambda_x s_y + \Lambda_y s_x \\ \Lambda_y s_y - \Lambda_x s_x\end{pmatrix}$	
E'_3	$\begin{pmatrix}-\Sigma_z\Lambda_y \\ \Sigma_z\Lambda_x\end{pmatrix}$, $\begin{pmatrix}-s_z\Lambda_y \\ s_z\Lambda_x\end{pmatrix}$	$\begin{pmatrix}\Lambda_x \\ \Lambda_y\end{pmatrix}$

under the reflection symmetry $z \to -z$ defined by the layer of transition-metal atoms

$$V^e(\mathbf{r}) = s_z \left[\sum_{n=x,y,z} \mathcal{U}^e_n(\mathbf{r})\Sigma_n + \sum_{l=x,y,z} \mathcal{V}^e_l(\mathbf{r})\Lambda_l \right],$$
$$V^o(\mathbf{r}) = \sum_{j=x,y} s_j \left[\sum_{n=x,y,z} \mathcal{U}^o_{jn}(\mathbf{r})\Sigma_n + \sum_{l=x,y,z} \mathcal{V}^o_{jl}(\mathbf{r})\Lambda_l \right]. \tag{B5}$$

Even terms conserve z spin, whereas odd terms induce spin flip. After projecting these terms onto a single band, we obtain for intervalley disorder potentials [Eq. (B4)]

$$V^{\text{int}}_{c,v}(\mathbf{r}) = \mathbf{V}_{c,v}(\mathbf{r}) \cdot \boldsymbol{\tau}, \quad \text{with}$$
$$V^x_{c,v}(\mathbf{r}) = V_{yy} \mp V_{xx} - \frac{\gamma}{\Delta}(\partial_y V_{zx} \pm \partial_x V_{zy}), \tag{B6}$$
$$V^y_{c,v}(\mathbf{r}) = -V_{yx} \mp V_{xy} - \frac{\gamma}{\Delta}(\partial_y V_{zy} \mp \partial_x V_{zx}).$$

Similarly, for even and odd spin-dependent disorder potentials [Eqs. (B5)] we arrive at

$$V^e_{c,v}(\mathbf{r}) = \left(\mathcal{V}^e_z \pm \mathcal{U}^e_z\right)\tau_z s_z + \frac{\gamma}{\Delta} s_z \left[\pm \{\mathbf{p}, \boldsymbol{\mathcal{U}}^e\} + [\nabla \times \boldsymbol{\mathcal{U}}^e]_z \tau_z + \left(\pm\{p_y, \mathcal{V}^e_y\} - \{p_x, \mathcal{V}^e_x\}\right)\tau_x - \left(\{p_x, \mathcal{V}^e_y\} \pm \{p_y, \mathcal{V}^e_x\}\right)\tau_y \right],$$
$$V^o_{c,v}(\mathbf{r}) = \sum_{j=x,y} s_j \Big\{ \left(\mathcal{V}^o_{jz} \pm \mathcal{U}^o_{jz}\right)\tau_z + \frac{\gamma}{\Delta}\left[\pm \{\mathbf{p}, \boldsymbol{\mathcal{U}}^o_j\} + \left[\nabla \times \boldsymbol{\mathcal{U}}^o_j\right]_z \tau_z + \left(\pm\{p_y, \mathcal{V}^o_{jy}\} - \{p_x, \mathcal{V}^o_{jx}\}\right)\tau_x \right. \tag{B7}$$
$$\left. - \left(\{p_x, \mathcal{V}^o_{jy}\} \pm \{p_y, \mathcal{V}^o_{jx}\}\right)\tau_y \right] \Big\}.$$

Equations (B6) and (B7) enable us to relate parameters in the phenomenological model for disorder in Eq. (1b) to their microscopic counterparts as

$$u_z(\mathbf{r}) = \mathcal{V}^e_z \pm \mathcal{U}^e_z + \frac{\gamma}{\Delta}[\nabla \times \boldsymbol{\mathcal{U}}^2]_z, \qquad \mathbf{a}_{gz} = \frac{\gamma}{\Delta}\boldsymbol{\mathcal{U}}^e, \qquad u^i_{sf} = \mathcal{V}^o_{iz} \pm \mathcal{U}^o_{iz} + \frac{\gamma}{\Delta}\left[\nabla \times \boldsymbol{\mathcal{U}}^o_i\right]_z,$$
$$\mathbf{w}_\alpha = \frac{\gamma}{\Delta}\boldsymbol{\mathcal{U}}^o_\alpha, \qquad \mathbf{u}_i = \mathbf{V}_{c,v}, \qquad \mathbf{w}_{zx} = \frac{\gamma}{\Delta}\left(-\mathcal{V}^e_x, \pm\mathcal{V}^e_y\right), \tag{B8}$$
$$\mathbf{w}_{zy} = \frac{\gamma}{\Delta}\left(-\mathcal{V}^e_y, \mp\mathcal{V}^e_x\right), \qquad \mathbf{w}_{\alpha x} = \frac{\gamma}{\Delta}\left(-\mathcal{V}^o_{\alpha x}, \pm\mathcal{V}^o_{\alpha y}\right), \qquad \mathbf{w}_{\alpha y} = \frac{\gamma}{\Delta}\left(-\mathcal{V}^o_{\alpha y}, \mp\mathcal{V}^o_{\alpha x}\right).$$

[1] X. Xu, W. Yao, D. Xiao, and T. F. Heinz, Nat. Phys. **10**, 343 (2014), and references therein.

[2] L. Britnell, R. M. Ribeiro, A. Eckmann, R. Jalil, B. D. Belle, A. Mishchenko, Y.-J. Kim, R. V. Gorbachev, T. Georgiou, S. V. Morozov, A. N. Grigorenko, A. K. Geim, C. Casiraghi, A. H. Castro Neto, and K. S. Novoselov, Science **340**, 1311 (2013).

[3] Andreas Pospischil, Marco M. Furchi, and Thomas Mueller, Nat. Nanotechnol. **9**, 257 (2014).

[4] Jason S. Ross, Philip Klement, Aaron M. Jones, Nirmal J. Ghimire, Jiaqiang Yan, D. G. Mandrus, Takashi Taniguchi, Kenji Watanabe, Kenji Kitamura, Wang Yao, David H. Cobden, and Xiaodong Xu, Nat. Nanotechnol. **9**, 268 (2014).

[5] Britton W. H. Baugher, Hugh O. H. Churchill, Yafang Yang, and Pablo Jarillo-Herrero, Nat. Nanotechnol. **9**, 262 (2014).

[6] Sanghyun Jo, Nicolas Ubrig, Helmuth Berger, Alexey B. Kuzmenko, and Alberto F. Morpurgo, Nano Lett. **14**, 2019 (2014).

[7] B. Radisavljevic, A. Radenovic, J. Brivio, V. Giacometti, and A. Kis, Nat. Nanotechnol. **6**, 147 (2011).

[8] D. Lembke and A. Kis, ACS Nano **6**, 10070 (2012).

[9] Han Wang, Lili Yu, Yi-Hsien Lee, Yumeng Shi, Allen Hsu, Matthew L. Chin, Lain-Jong Li, Madan Dubey, Jing Kong, and Tomás Palacios, Nano Lett. **12**, 4674 (2012).

[10] Hui Fang, Steven Chuang, Ting Chia Chang, Kuniharu Takei, Toshitake Takahashi, and Ali Javey, Nano Lett. **12**, 3788 (2012).

[11] Dattatray J. Late, Bin Liu, H. S. S. Ramakrishna Matte, Vinayak P. Dravid, and C. N. R. Rao, ACS Nano **6**, 5635 (2012).

[12] Wei Liu, Jiahao Kang, Deblina Sarkar, Yasin Khatami, Debdeep Jena, and Kaustav Banerjee, Nano Lett. **13**, 1983 (2013).

[13] Jiahao Kang, Wei Liu, and Kaustav Banerjee, Appl. Phys. Lett. **104**, 093106 (2014).

[14] Saptarshi Das, Richard Gulotty, Anirudha V. Sumant, and Andreas Roelofs, Nano Lett. **14**, 2861 (2014).

[15] Youngki Yoon, Kartik Ganapathi, and Sayeef Salahuddin, Nano Lett. **11**, 3768 (2011).

[16] Britton W. H. Baugher, Hugh O. H. Churchill, Yafang Yang, and Pablo Jarillo-Herrero, Nano Lett. **13**, 4212 (2013).

[17] B. Radisavljevic and Andras Kis, Nat. Mater. **12**, 815 (2013).

[18] Deep Jariwala, Vinod K. Sangwan, Dattatray J. Late, James E. Johns, Vinayak P. Dravid, Tobin J. Marks, Lincoln J. Lauhon, and Mark C. Hersam, Appl. Phys. Lett. **102**, 173107 (2013).

[19] Wanxiang Feng, Yugui Yao, Wenguang Zhu, Jinjian Zhou, Wang Yao, and Di Xiao, Phys. Rev. B **86**, 165108 (2012).

[20] Dmitry Ovchinnikov, Adrien Allain, Ying-Sheng Huang, Dumitru Dumcenco, and Andras Kis, ACS Nano **8**, 8174 (2014).

[21] Rafael Roldán, Jose A. Silva-Guillén, M. Pilar, López-Sancho, Francisco Guinea, Emmanuele Cappelluti, and Pablo Ordejón, Ann. Phys. (Berlin) **526**, 347 (2014), and references therein.

[22] D. Xiao, G.-B. Liu, W. Feng, X. Xu, and W. Yao, Phys. Rev. Lett. **108**, 196802 (2012).

[23] Z. Y. Zhu, Y. C. Cheng, and U. Schwingenschlögl, Phys. Rev. B **84**, 153402 (2011).

[24] Alejandro Molina-Sánchez, Davide Sangalli, Kerstin Hummer, Andrea Marini, and Ludger Wirtz, Phys. Rev. B **88**, 045412 (2013).

[25] Andor Kormányos, Viktor Zólyomi, Neil D. Drummond, Péter Rakyta, Guido Burkard, and Vladimir I. Fal'ko, Phys. Rev. B **88**, 045416 (2013).

[26] S. K. Mahatha, K. D. Patel, and K. S. R. Menon, J. Phys.: Condens. Matter **24**, 475504 (2012).

[27] Wencan Jin, Po-Chun Yeh, Nader Zaki, Datong Zhang, Jerzy T. Sadowski, Abdullah Al-Mahboob, Arend M. van der Zande, Daniel A. Chenet, Jerry I. Dadap, Irving P. Herman, Peter Sutter, James Hone, and Richard M. Osgood Jr., Phys. Rev. Lett. **111**, 106801 (2013).

[28] Kin Fai Mak, Changgu Lee, James Hone, Jie Shan, and Tony F. Heinz, Phys. Rev. Lett. **105**, 136805 (2010).

[29] Won Seok Yun, S. W. Han, Soon Cheol Hong, In Gee Kim, and J. D. Lee, Phys. Rev. B **85**, 033305 (2012).

[30] M. L. Mehta, *Random Matrices* (Academic Press, New York, 1991).

[31] A. Altland and M. R. Zirnbauer, Phys. Rev. B **55**, 1142 (1997).

[32] B. L. Altshuler, D. Khmel'nitzkii, A. I. Larkin, and P. A. Lee, Phys. Rev. B **22**, 5142 (1980).

[33] S. Hikami, A. I. Larkin, and Y. Nagaoka, Prog. Theor. Phys. **63**, 707 (1980).

[34] S. V. Iordanskii and A. E. Koshelev, Pis'ma Zh. Eskp. Teor. Fiz. **41**, 471 (1985) [JETP Lett. **41**, 574 (1985)].

[35] A. F. Morpurgo and F. Guinea, Phys. Rev. Lett. **97**, 196804 (2006).

[36] E. McCann, K. Kechedzhi, Vladimir I. Falko, H. Suzuura, T. Ando, and B. L. Altshuler, Phys. Rev. Lett. **97**, 146805 (2006).

[37] K. Kechedzhi, Vladimir I. Falko, E. McCann, and B. L. Altshuler, Phys. Rev. Lett. **98**, 176806 (2007).

[38] Hai-Zhou Lu, Wang Yao, Di Xiao, and Shun-Qing Shen, Phys. Rev. Lett. **110**, 016806 (2013).

[39] A. Kuc, N. Zibouche, and T. Heine, Phys. Rev. B **83**, 245213 (2011).

[40] H. P. Komsa and A. V. Krasheninnikov, Phys. Rev. B **86**, 241201 (2012).

[41] We neglect a possible effective mass difference [25] between two Kramers doublets $(K_+,\uparrow;K_-,\downarrow)$ and $(K_+,\downarrow;K_-,\uparrow)$.

[42] Andor Kormányos, Guido Burkard, Martin Gmitra, Jaroslav Fabian, Viktor Zólyomi, Neil D. Drummond, and Vladimir Fal'ko, arXiv:1410.6666.

[43] H. Ochoa, F. Guinea, and V. I. Fal'ko, Phys. Rev. B **88**, 195417 (2013).

[44] For spinful electrons at valleys $K_\pm$ time inversion is implemented by the antiunitary operator $\mathcal{T} = is_y\tau_x\mathcal{K}$, where $\mathcal{K}$ stands for complex conjugation. Therefore, $s_i\tau_j \xrightarrow{\mathcal{T}} -s_i\tau_j$ for $i,j = x,y$. As consequence, terms in the Hamiltonian that could simultaneously flip spin and scatter an electron in the same Wannier state between K_+ and K_- are forbidden since their appearance would require breaking time-inversion symmetry, as it is deduced from Table I. More generally, time-inversion symmetry forbids spin-flip scattering of electrons in the same Wannier state between any pair of opposite points in the Brillouin zone. An illustration of this general statement, given in Ref. [45], appeals to a free 2D electron scattering off a potential $V(\mathbf{r})$, for SO coupling is described by $\mathcal{H}_{\rm SO} \propto [\boldsymbol{\nabla} V(\mathbf{r}) \times \mathbf{p}] \cdot \mathbf{s}$. For such a perturbation, spin-flip scattering has an amplitude $\langle \mathbf{k}\alpha|\mathcal{H}_{\rm SO}|\mathbf{k}'\beta\rangle \propto i(\mathbf{k}\times\mathbf{k}')\cdot[\mathbf{s}]_{\alpha\beta} V(\mathbf{k}-\mathbf{k}')$, which vanishes for the pairs of states related by the time-inversion transformation [$V(\mathbf{q})$ is the Fourier transform of $V(\mathbf{r})$]. Hence, $|\langle -\mathbf{k}-\alpha|\mathcal{H}_{\rm SO}|\mathbf{k}\beta\rangle|^2 \equiv 0$.

[45] Y. Yafet, *Solid State Physics* (Academic Press, New York, 1963).

[46] Hongtao Yuan, Mohammad Saeed Bahramy, Kazuhiro Morimoto, Sanfeng Wu, Kentaro Nomura, Bohm-Jung Yang, Hidekazu Shimotani, Ryuji Suzuki, Minglin Toh, Christian Kloc, Xiaodong Xu, Ryotaro Arita, Naoto Nagaosa, and Yoshihiro Iwasa, Nat. Phys. **9**, 563 (2013).

[47] Adam T. Neal, Han Liu, Jiangjiang Gu, and Peide D. Ye, ACS Nano **7**, 7077 (2013).

[48] K. Kechedzhi, O. Kashuba, and V. I. Falko, Phys. Rev. B **77**, 193403 (2008).

[49] With this choice, time inversion is implemented by the antiunitary operator $\mathcal{T} = i\sigma_y\mathcal{K}$.

[50] Note that under the assumption $\tau/\tau_0 \sim 1$ the dressed Hikami box diagrams do not contribute. The velocity operators at each external vertex of these diagrams carry different momentum, and therefore they average to zero separately when evaluating the angular part of the integrals if the disorder correlator has no extra momentum dependence in order to compensate this, as it happens with diagonal disorder. This is no longer true for *gauge* disorder. However, given that $\tau_g^{-1} \propto n$, we can assume that $\tau_0^{-1} \gg \tau_g^{-1}$ and neglect the contribution from dressed Hikami boxes.

[51] I. L. Aleiner and V. I. Fal'ko, Phys. Rev. Lett. **87**, 256801 (2001).

[52] E. McCann and V. I. Falko, Phys. Rev. Lett. **108**, 166606 (2012).

[53] S. Maekawa and H. Fukuyama, J. Phys. Soc. Jpn. **50**, 2516 (1981).

[54] H. Ochoa and R. Roldán, Phys. Rev. B **87**, 245421 (2013).

[55] K. F. Mak, K. He, J. Sahn, and T. F. Heinz, Nat. Nanotechnol. **7**, 494 (2012).

[56] Y. A. Bychkov and E. I. Rashba, J. Phys. C: Solid State Phys. **17**, 6039 (1984).

[57] M. I. Dyakonov and V. I. Perel, Fiz. Tverd. Tela **13**, 3581 (1971) [Sov. Phys.–Solid State **13**, 3023 (1971)].

[58] M. I. Dyakonov, *Spin Physics in Semiconductors* (Springer, Berlin, 2008).

[59] J. B. Miller, D. M. Zumbühl, C. M. Marcus, Y. B. Lyanda-Geller, D. Goldhaber-Gordon, K. Campman, and A. C. Gossard, Phys. Rev. Lett. **90**, 076807 (2003).

[60] Jan-Hein Cremers, Piet W. Brouwer, and Vladimir I. Falko, Phys. Rev. B **68**, 125329 (2003).

[61] Note that Δ refers to the band gap, not to the spin splitting of the bands λ.

[62] This is the Berry curvature deduced from the $\mathbf{k}\cdot\mathbf{p}$ Hamiltonian neglecting warping effects.

[63] J. R. Schrieffer and P. A. Wolf, Phys. Rev. **149**, 491 (1966).